Available online at www.sciencedirect.com
ScienceDirect
Trans. Nonferrous Met. Soc. China 29(2019) 460−472
Transactions of Nonferrous Metals Society of China
www.tnmsc.cn

Improving mechanical properties of Mn-added hypoeutectic Al−4Ni alloy by friction stir processing

Fatemeh YOUSEFI, Reza TAGHIABADI, Saeid BAGHSHAHI

Department of Materials Science and Metallurgy, Imam Khomeini International University (IKIU), Qazvin, Iran

Received 5 May 2018; accepted 16 November 2018

Abstract: The effects of Mn addition (1 wt.%, 2 wt.% and 4 wt.%) and friction stir processing (FSP) on the microstructure and mechanical properties of Al−4Ni alloy were studied. The results showed that Mn promoted the formation of Al_6Mn and $Al_{60}Mn_{11}Ni_4$ intermetallics. These Mn-rich compounds increased the strength and hardness, but decreased the ductility and fracture toughness of the alloy. To improve the ductility and toughness, the as-cast alloys were then subjected to FSP (rotation speed of 1600 r/min and traverse speed of 12 mm/min). According to the results, FSP greatly improved the mechanical properties. The tensile strength, yield strength, fracture strain, microhardness, and fracture toughness of FSPed Al−4Ni−2Mn increased by 67%, 30%, 230%, 20%, and 1185%, respectively. The fine redistribution of Mn-rich compounds, formation of ultrafine grains, microstructural densification, and the elimination of casting defects such as micropores and oxide bifilms were found to be the most important factors responsible for improving the mechanical properties. The fractographic investigations also revealed that the fracture of as-cast Mn-rich alloys changed from the brittle mode containing micro-facets to a more ductile fracture mode containing fine and equiaxed dimples in FSPed alloys.

Key words: friction stir processing; Al−Ni alloy; manganese; intermetallics; mechanical properties

1 Introduction

Al−Si casting alloys are widely used in several engineering applications due to their specific advantages including low density, excellent castability, good tribological properties, etc. [1−3]. These alloys, however, suffer from poor strength at working temperatures above 300 °C [4]. Their inferior high-temperature resistance is thought to be due to the dissolution and/or coarsening of the strengthening phases or the liquation of low-melting-point constituents in inter-dendritic regions [5,6]. It has been reported that the presence of alloying elements like Mg, Cu and Zn reduces the alloy liquidus temperature and, due to their relatively high diffusivity in α(Al) matrix, further weakens the alloy at high temperatures [4,7].

In this regard, many attempts have been made to develop new classes of alloys with better high-temperature properties than Al−Si alloys. One of the most promising alloy groups being developed is the alloy based on Al−Ni eutectic system (6.1 wt.% Ni and 640 °C) [8,9]. Due to the higher solidus temperature and the presence of thermally stable Al_3Ni intermetallics (melting point=854 °C) in their microstructure, Al−Ni-based alloys show improved mechanical properties at room and elevated temperatures (up to 500 °C) [7,10]. Moreover, these alloys show excellent fluidity, great feeding ability, and very low susceptibility to hot-tearing [11,12]. In addition, contrary to the eutectic Si particles in the microstructure of Al−Si alloys, the Al−Al_3Ni interfacial bonding is strong leading to a more efficient inter-phase load transfer and lower microcracking probability [13].

Mechanical properties of binary Al−Ni alloys, however, are not high enough to meet the requirements of most engineering applications [9,14]. Therefore, a large number of studies have been conducted to increase their mechanical strength through individual or combined effects of alloying elements, heat treatment, and high cooling rate [9,15−19]. Mn has been one of the most common alloying additions to Al−Ni alloys which is mainly crystallized as Al_6Mn dispersoids in the matrix [9]. According to previous findings, Al−Ni−Mn alloys can have comparable or even higher mechanical properties than commercial A356 alloys, especially at

Corresponding author: Reza TAGHIABADI; E-mail: taghiabadi@ikiu.ac.ir
DOI: 10.1016/S1003-6326(19)64955-1

elevated temperatures [8]. Improved high-temperature mechanical properties of Al−Ni−Mn alloys are attributed to the presence of Al_6Mn precipitate that is coarsened by a much slower rate than common Al_2Cu and Mg_2Si precipitates present in the microstructure of Al−Si−Mg (Cu) or Al−Cu alloys [9,20].

However, due to the limited solid solubility of Mn in Al (max. 1.2 wt.% at 659 °C), a low amount of Al_6Mn precipitates can form during aging treatment (max. 5.8 wt.%), thereby the highest attainable strength in Al−Ni−Mn alloys is limited [9]. Moreover, formation of hard Al_3Ni and Al_6Mn intermetallics increases mechanical strength, but reduces alloy ductility making it unsuitable for most engineering applications [21]. Therefore, it seems necessary to adopt a practical approach to overcome these drawbacks.

Recently, FAN et al [9] proposed a novel heat treatment process to refine the intermetallics and increase the yield strength of Al−6Ni−(2−4)Mn alloys. The samples were first solidified under a high cooling rate (~90 °K/s) and then subjected to an aging process. The rapid solidification produces a supersaturated solid solution containing much more amounts of Mn when compares to traditional heat treatment. GONZALEZ et al [21], investigated the effect of melt spinning on the microstructure and hardness of Al−4Ni alloy, and showed that the formation of fine and globular Al_9Ni_2 and Al_3Ni intermetallics enhanced the alloy hardness from HV 58 to HV 371. FAN et al [9] proposed Zr and V micro-alloying (mole ratio Zr:V=1:4) to improve the mechanical properties of Al−Ni alloy at low and high temperatures (300 °C).

Severe plastic deformation (SPD) techniques are widely used for producing ultrafine-structured metallic materials with great tensile strength and good tensile ductility and toughness. SPD techniques are specially used for microstructural modification of Al alloys. This is because high stacking fault energy of Al limits its effective refinement through thermo-mechanical induced recrystallization. FSP, developed by MA [22], GAN et al [23], CHEN et al [24], MISHRA and MA [25], is a new SPD technique capable of microstructural modification. In FSP, a specially-designed shouldered tool is plunged into the material surface until its shoulder touches the material surface. The tool starts rotating until the desired temperature and plasticity are obtained through frictional heating and material mixing. The rotating tool then moves along the surface in a desired direction and simultaneously promotes the refinement, homogenization, and densification of the material in the processing area [25,26]. Due to significant improvements in material properties, FSP has attracted numerous research interests. However, to the best of our knowledge, there are no systematic experimental data addressing with the FSP of Al−Ni−Mn alloys. Therefore, the aim of this study is to investigate the effect of FSP on the microstructure and mechanical properties of Al−4Ni−(1−4)Mn alloys.

2 Experimental

Table 1 shows the code and chemical composition of Al−Ni−*x*Mn alloys used in this study. The alloys were prepared by melting high-purity Al (99.9%) in a SiC crucible using an induction melting furnace (3400 V, 50 Hz, 60 kW) under the protection of high-purity argon atmosphere (99.999 wt.%). Desired amounts of Ni and Mn were added to the liquid Al using high purity Ni (99.96 wt.%) and Al−30Mn master alloys, respectively. Then, the melt was superheated up to 780 °C, grain refined by the addition of 0.2 wt.% Ti using Al−6Ti master alloy, stirred gently, and poured into a preheated (250 °C) cast-iron mold (Fig. 1) to obtain an ingot of 170 mm×100 mm×8 mm in size. The average cooling rate of the mold was 4.8 °C/s.

The FSP tool used in this study was a cylindrical pin made of AISI H13 tool steel (hardened and tempered to HRC (58±2)) with a diameter of 5 mm, height of 5 mm,

Table 1 Alloy code and mass fraction of main alloying elements in alloys studied (wt.%)

Alloy code	Sample condition	Ni	Mn
4Ni	As-cast	4.11	<0.01
4Ni1Mn	As-cast	4.14	0.96
4Ni2Mn	As-cast	4.08	2.02
4Ni4Mn	As-cast	4.03	4.14
4NiF	FSPed	3.94	<0.01
4Ni1MnF	FSPed	3.97	1.04
4Ni2MnF	FSPed	4.15	2.06
4Ni4MnF	FSPed	4.03	4.11

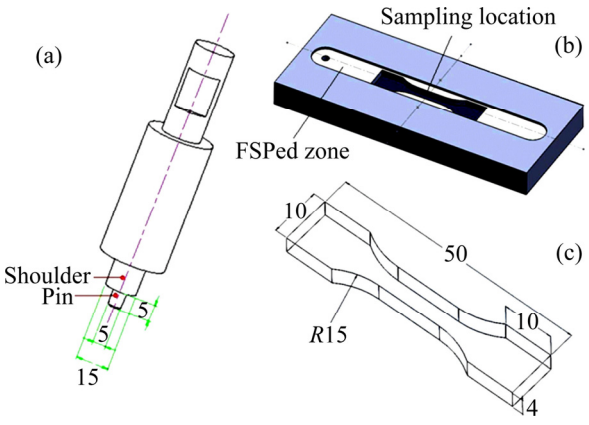

Fig. 1 Schematic diagram of FSP tool (a), tensile test sampling location (b), and geometry and dimensions (c) of tensile test specimen (Unit: mm)

and shoulder diameter of 15 mm. The tool shape and its dimensions are shown in Fig. 1(a). The FSP was carried out using a XIOS-ZAYER milling machine under the optimized process parameters, i.e. constant traverse speed of 12 mm/min and rotation speed of 1600 r/min.

The tensile specimens with the dimension shown in Figs. 1(b) and (c) were machined out from the processed zone parallel to the FSP direction and tested by a Zwick/Roell-Z100 universal tensile testing machine at the constant crosshead speed of 0.5 mm/min. The Vickers micro-hardness tests were performed by a Gnehm-Härteprüfer FM100 micro-hardness tester with a load of 500 g for 15 s on the transverse cross-section of FSPed zone at the mid-thickness of the plates. Samples for metallographic observations were prepared by standard metallographic procedures and each cross-section was etched using 2%HF−distilled water reagent. Some of the specimens were also etched by diluted Keller's reagent (2 mL HF, 5 mL HCl, 3 mL HNO_3, and 190 mL distilled H_2O) for macrostructural observations. The microstructure of the specimens was examined by an Olympus (BX51M) OM and a Tescan-Vega SEM equipped with an energy dispersive spectroscopy (EDS). The fracture surface of the tensile specimens was also studied by the SEM. The average size of grains was also evaluated as per ASTM E112 by the linear intercept method. Quantitative metallography was also carried out using UTHSCSA image tool (Ver. 1.28).

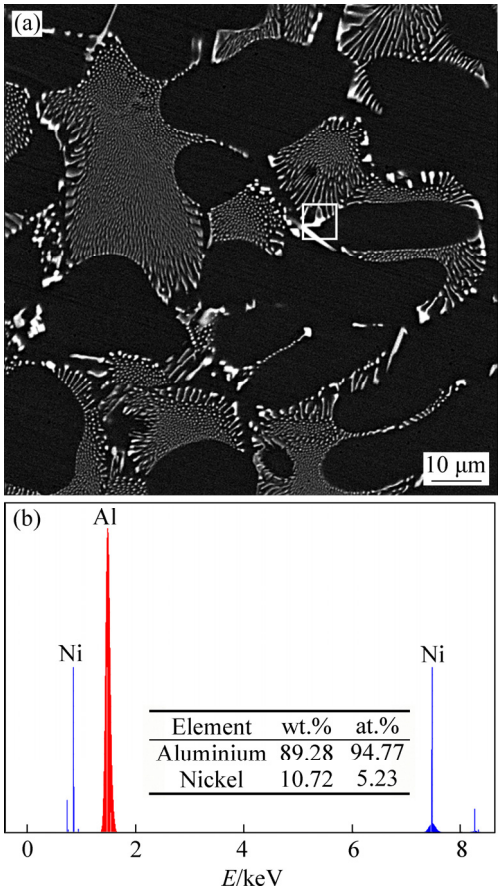

Fig. 2 SEM image of base alloy (Al−4Ni) (a), and EDS analysis (b) of Al_3Ni phase shown in micrograph (a)

3 Results and discussion

3.1 Microstructural characterization

The as-cast microstructure of 4Ni (base) alloy is shown in Fig. 2(a). As seen, the microstructure is mainly composed of α(Al) dendrites (dark-gray regions) and α(Al)/Al_3Ni eutectic (bright regions). The EDS spectrum of the eutectic Al_3Ni phase is also presented in Fig. 2(b). The Mn addition leads to the precipitation of Mn-rich intermetallic compounds in the matrix (Fig. 3), and their typical EDS analyses are shown in Table 2. According to the XRD patterns (Fig. 4), the main Mn-rich phases in the microstructure of Mn-bearing alloys are Al_6Mn and $Al_{60}Mn_{11}Ni_4$ (*O*-phase). However, it is very hard to observe Al_6Mn phases in the microstructure. This is probably due to the fact that the high consumption of Mn during primary *O*-phase formation decreases the supersaturation degree of Mn solid-solution [9] leading to a very low volume fraction of fine Al_6Mn particles. It is also evident from Fig. 3 that both the effective size and volume fraction of Mn-rich compounds increase with Mn concentration in the alloy.

The morphology and distribution of Mn-rich compounds are also dependent on Mn concentration. The Mn-rich compounds in the microstructure of 4Ni1Mn alloy were mostly precipitated as fine inter-dendritic particles (Fig. 3(a)). With increasing the Mn content, the size and volume fraction of particles increase in a way that they appear as larger blocky-shape and needle-like particles in 4Ni4Mn sample.

Figure 5 depicts the effect of FSP on the microstructure of Al−4Ni−2Mn and Al−4Ni−4Mn alloys. As can be seen, due to high frictional heating and intense plastic strains applied during the FSP [25,26], FSPed samples exhibit a homogenous microstructure comprised of finely distributed second-phase particles in the matrix, which have less density of micro-pores. The effect of FSP on reducing the microporosities and refining second-phase intermetallics can be also well evaluated from the image analysis results, in which the volume fraction of micropores and the average size of the primary particles in 4Ni4Mn sample decreased from (3.11±1.62) and (47.18±9.29) μm in as-cast condition to (0.64±0.11) and (2.75±2.26) μm in FSPed condition.

FSP also promotes the formation of ultrafine-grain α(Al) in the processed zone. Figure 6 shows the effect of FSP on the grain structure of 4Ni4MnF sample. As seen, a drastic reduction of the grain size is observed in the stir

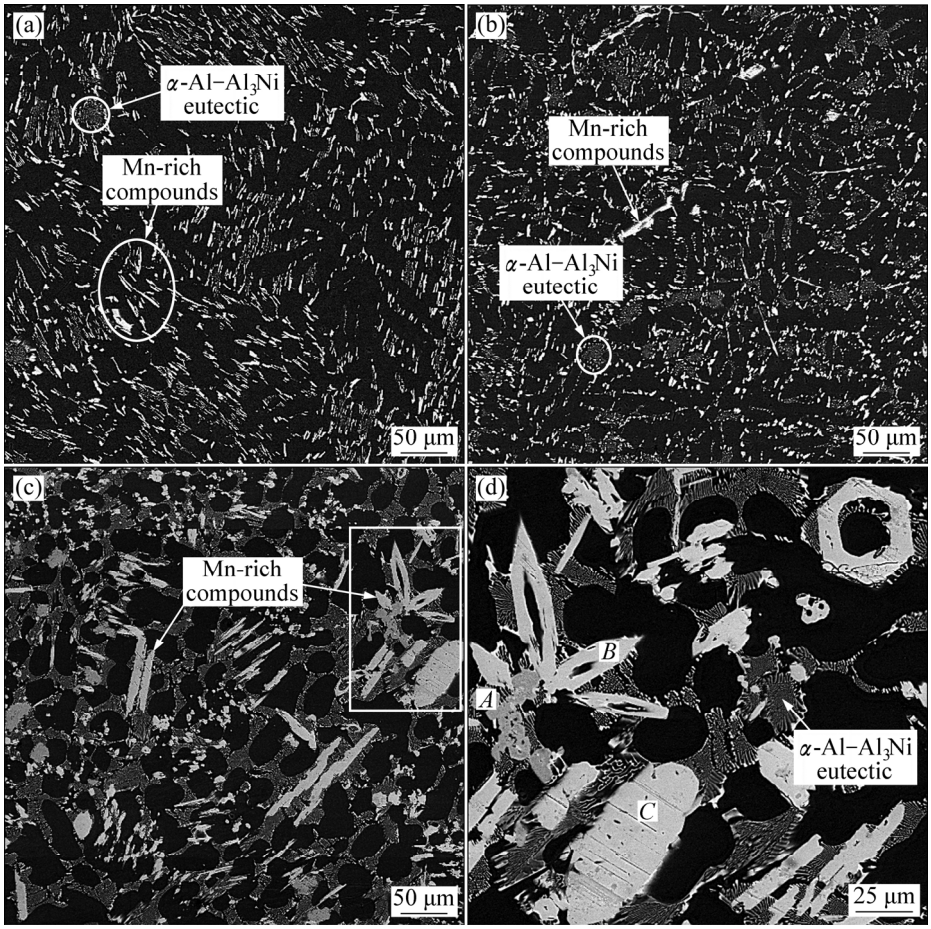

Fig. 3 SEM images showing microstructure of Mn-containing alloys: (a) 4Ni1Mn; (b) 4Ni2Mn; (c) 4Ni4Mn; (d) Higher magnification of 4Ni4Mn alloy (boxed area in Fig. 3(c))

Table 2 EDS analyses of Mn-rich phases shown in Fig. 3(d)

Phase code in Fig. 3(d)	Chemical composition/at.%			
	Al	Ni	Mn	Ti
A	84.66	1.66	12.62	1.07
B	79.85	3.12	16.72	0.30
C	82.85	2.58	14.57	–

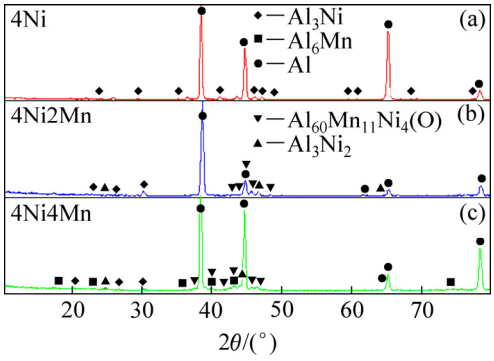

Fig. 4 XRD patterns of 4Ni (a), 4Ni2Mn (b), and 4Ni4Mn (c) alloys

zone (SZ), where their average size reduced from (513.7±146.3) μm in the base metal to less than (1.14±0.90) μm in the SZ. This reduction can be related to the severe plastic deformation and dynamic recrystallization through the process [22,23,25−29]. The size of grains in the SZ can be predicted by the following equation [27]:

$$d^{-1} = a + b \lg Z \tag{1}$$

where d is the grain diameter, and a and b are the material constants. The Zener parameter (Z) is given by

$$Z = \dot{\varepsilon} \exp \frac{Q}{RT} \tag{2}$$

where $\dot{\varepsilon}$ is the strain rate, Q is the activation energy, T is the temperature, and R is the gas constant.

3.2 Mechanical properties

The engineering stress−strain curves corresponding to the base and FSPed samples containing different amounts of Mn are presented in Fig. 7. As seen, Mn

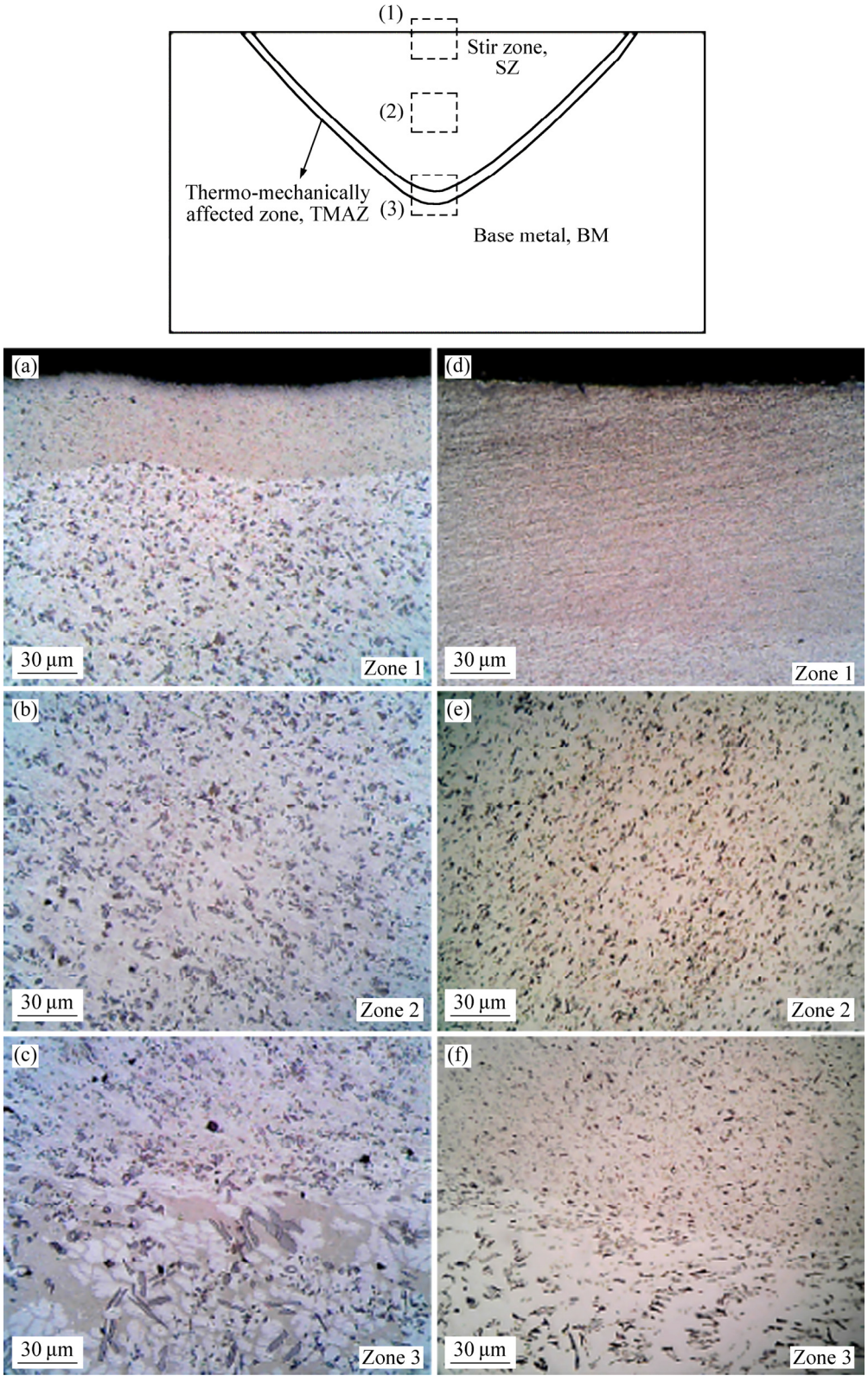

Fig. 5 OM micrographs showing microstructure of different regions of FSPed area: (a−c) 4Ni2Mn alloy; (d−f) 4Ni4Mn alloy

addition relatively increases the yield and tensile strength, but substantially decreases the fracture strain of the as-cast Al−4Ni alloy. In contrast, FSP significantly increases the yield and the tensile strength, and the tensile ductility of the alloy.

The effects of Mn addition on the tensile strength, yield strength, fracture strain, fracture toughness, and micro-hardness of Al−4Ni−*x*Mn alloys in as-cast and FSPed conditions are shown in Fig. 8. It is obvious from Figs. 8(a) and (b) that Mn addition up to 4 wt.%

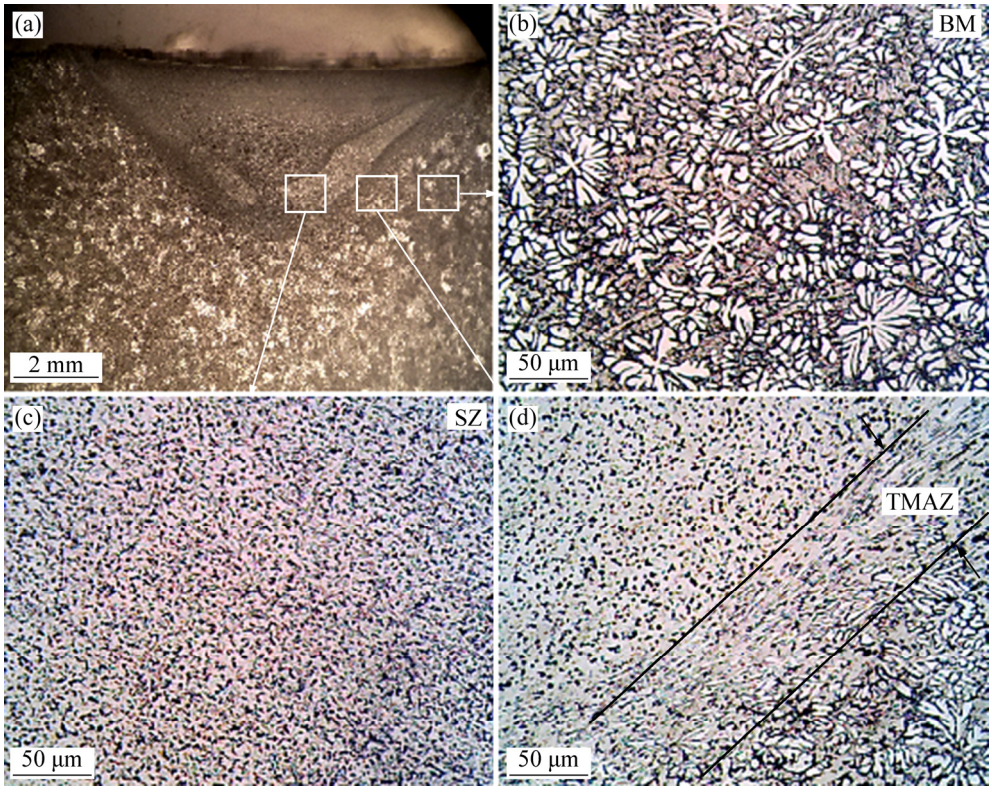

Fig. 6 Stereo microscope micrograph (a) showing grain structure of FSPed area and base metal in Al−4Ni alloy and OM micrographs (b−d) showing magnified microstructure of boxed areas in (a)

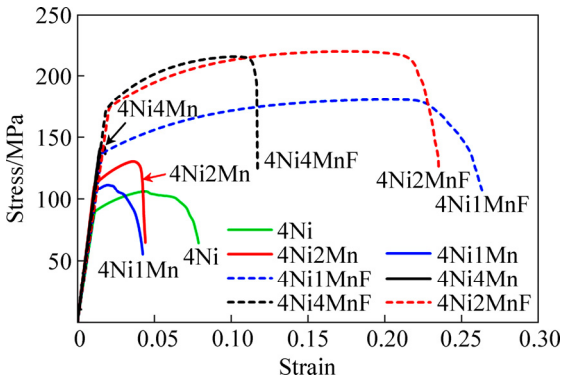

Fig. 7 Engineering stress−strain curves of experimental alloys containing different amounts of Mn in as-cast and FSPed conditions

increases the tensile and yield strength of the base alloy by 62% and 38%, respectively. The increasing rate, however, reduces after about 2 wt.% Mn. The effects of Mn on fracture strain and fracture toughness of Al−4Ni alloy are also shown in Figs. 8(d) and (e). As seen, Mn exerts negative impact on both the as-cast ductility and toughness of the alloy, especially in excess of 2 wt.%. According to the results, the fracture strain and fracture toughness of 4Ni4Mn sample are lower than those of 4Ni sample by 76% and 72%, respectively.

The positive effect of Mn on the strength and micro-hardness of Al−4Ni alloy can be explained by its solid-solution strengthening effect as well as the impeding action of Mn-rich intermetallic dispersoids on dislocations movement.

The solid solution strengthening (σ_{ss}) is commonly described by Eq. (3) [30−32]:

$$\sigma_{ss} = \sigma_{pure} + HC^n \quad (3)$$

where σ_{pure} is the yield stress of the pure matrix, H and n are constants, and C is the concentration of solute atom in at.%. Therefore, Mn addition, as it is expected, increases the alloy strength by solid solution mechanism. Solid solution strengthening arises from the interaction of dislocation elastic strain fields with the strain fields generated around the Mn solute atoms or their clusters with impurities [33]. These strain fields, which are believed to be originated from the atomic size misfit and/or the change in the matrix shear modulus caused by the solute atoms, arrest the dislocations motion and accordingly improve the strength.

The interaction of dislocations with intermetallic dispersoids also reduces their mean free path and promotes their rapid pileup [27] leading to the matrix strengthening by Orowan bowing mechanism. The Orowan strengthening is also generally approximated by Ashby−Orowan equation [34]:

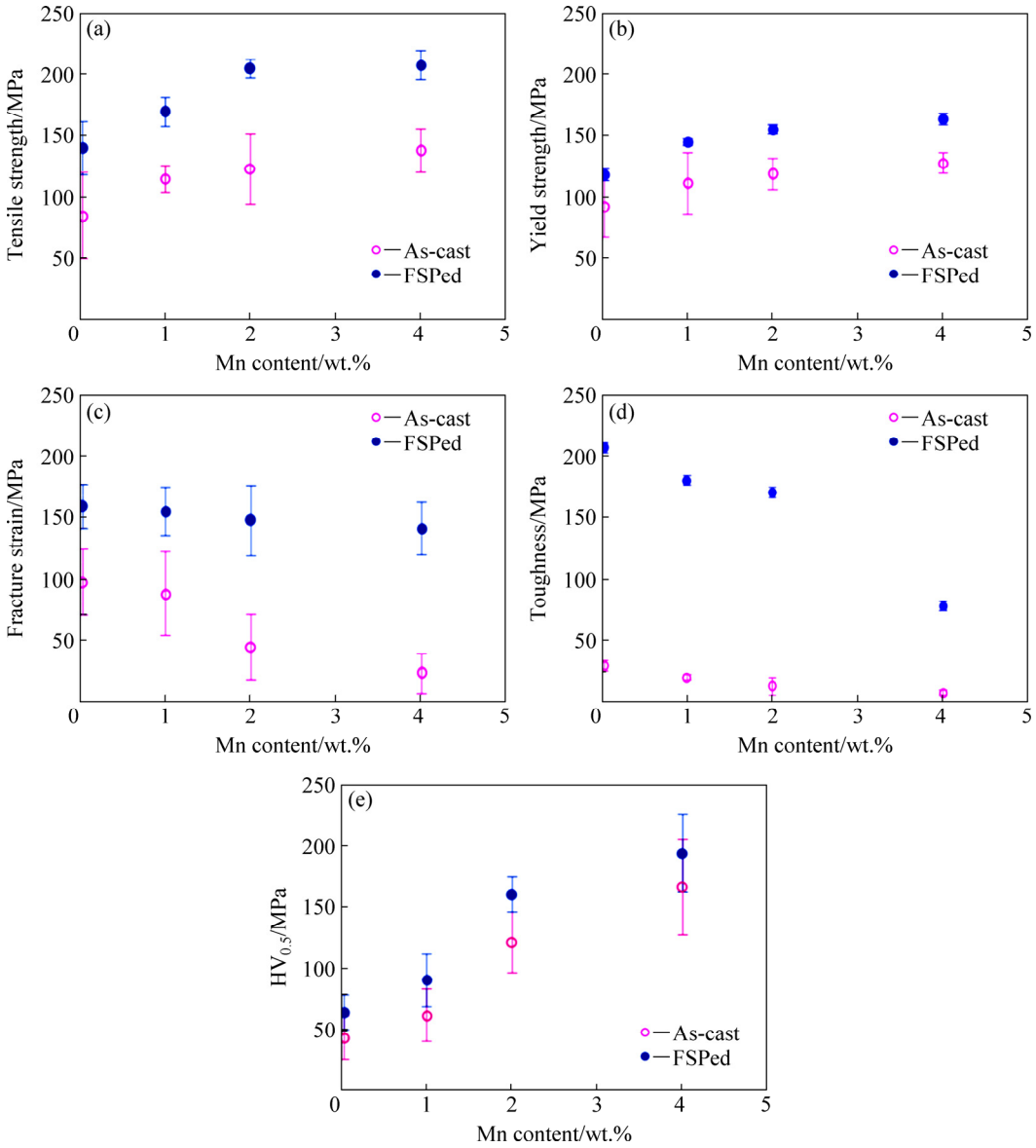

Fig. 8 Variation of tensile strength (a), yield strength (b), fracture strain (c), fracture toughness (d), and micro-hardness (e) of experimental alloys with different Mn contents

$$\sigma_{\mathrm{D}}=\frac{0.84MGb}{2\pi(1-\nu)^{0.5}\lambda}\ln\left(\frac{r}{b}\right) \tag{4}$$

where G is the shear modulus of the matrix, b is the Burgers vector of dislocations, M is the Taylor factor, and ν is the Poison ratio. The interspacing of the dispersoids (λ) is given by Eq. (5):

$$\lambda=r\left(\frac{2\pi}{3f}\right)^{0.5} \tag{5}$$

where r and f are the average radius and volume fraction of dispersoids, respectively.

However, Mn addition exerts negative impact on fracture strain and fracture toughness of the alloys (Figs. 8(c) and (d)). Based on the microstructural characteristics of the alloys (Fig. 3), the formation of large primary Mn-rich compounds can be considered as the main reason for the reduction of alloy ductility and fracture toughness. These intermetallics are brittle in nature and have weak faceted interface with the matrix [35]. Therefore, at a given applied load, they are likely to be fractured and/or debonded from the matrix much more easily facilitating the initiation and propagation of microcracks.

The critical role of large Mn-rich precipitates in the premature fracture of cast Al−4Ni alloys can be well investigated by fracture surface analysis. Figure 9 depicts the SEM micrographs of 4Ni1Mn and 4Ni4Mn samples in as-cast condition. As seen, the fracture surface of 4Ni1Mn alloy (Figs. 9(a, b) shows a quasi-cleavage fracture mode comprising of limited dimpled areas and cleavage micro-facets originated from the intermetallic

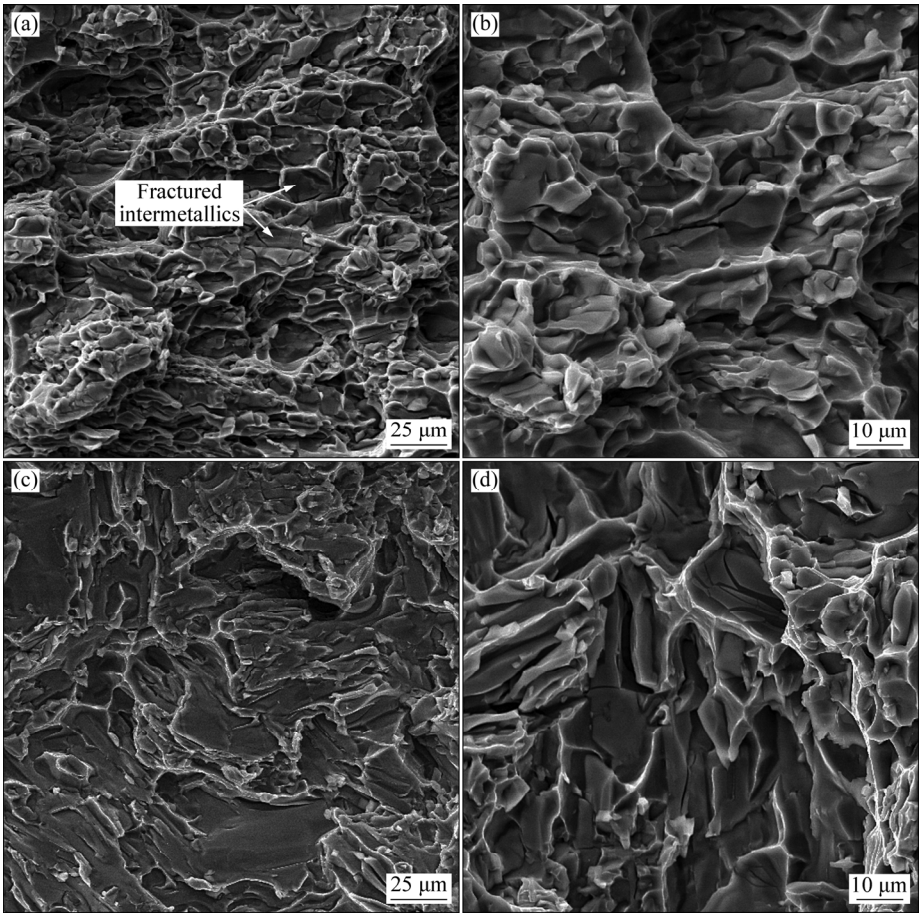

Fig. 9 SEM micrographs of fracture surfaces of 4Ni1Mn (a, b) and 4Ni4Mn (c, d) alloys

compounds. However, the fracture surface of 4Ni4Mn alloy (Figs. 9(c, d) exhibits large cleavage facets which are the indicators of brittle fracture.

In accordance with the results of microstructural investigation (Figs. 3(c, d), the extensive formation of micro-facets can be due to the presence of high volume fractions of brittle intermetallic compounds, especially the large primary Mn-rich intermetallics in the microstructure (Figs. 9 and 10). These phases, due to their large size and special morphology, are likely to act as potential stress concentrators when subjected to tensile loading, and, due to their brittle nature and weak bond strength with the matrix [35], serve as micro-crack initiators (Fig. 11(a)).

FSP significantly improves the strength, micro-hardness, ductility and fracture toughness of Al−4Ni−*x*Mn alloys. According to Fig. 8, the tensile strength, yield strength, fracture strain, microhardness, and fracture toughness of 4Ni4MnF sample have increased by 51%, 28%, 495%, 12%, and 850%, respectively, compared to those of 4Ni4Mn alloy, and by 145%, 77%, 44%, 130%, and 162%, respectively, compared to those of the as-cast base sample (4Ni). 4Ni2MnF has the optimum combination of mechanical

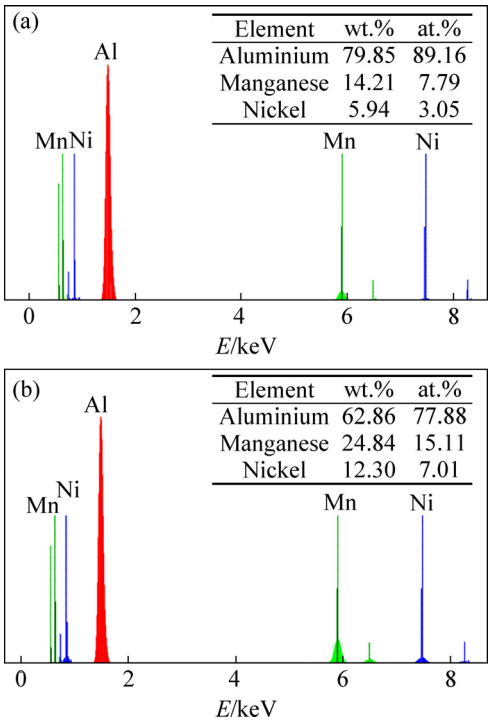

Fig. 10 EDS analyses of fractured intermetallics present on fracture surfaces of 4Ni4Mn (a) and 4Ni4MnF (b)

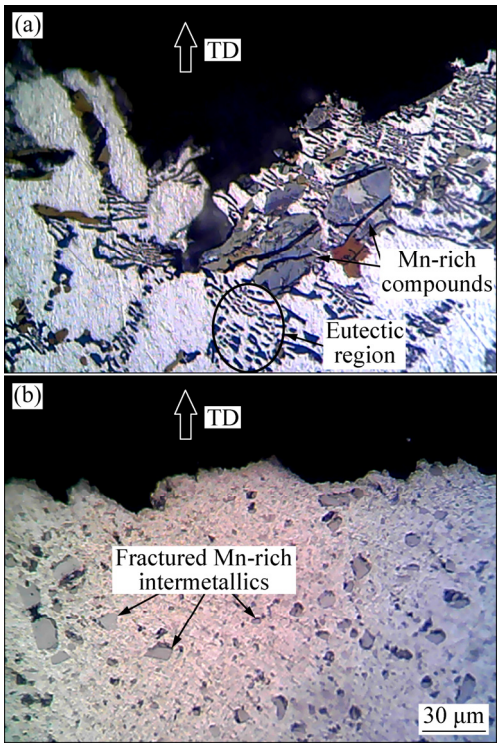

Fig. 11 OM micrographs taken from subsurface regions of fractured surfaces: (a) 4Ni4Mn showing initiation of micro-cracks from large Mn-rich intermetallics; (b) 4Ni4MnF alloys (TD stands for tensile direction)

properties compared to 4Ni, and its tensile strength, yield strength, fracture strain, microhardness, and fracture toughness have increased by 140%, 67%, 50%, 102%, and 470%, respectively.

According to the results of microstructure characterization (Figs. 3, 5 and 6), different mechanisms seem to be involved in the overall mechanical properties improvement of FSPed samples including formation of ultrafine-grained structure, breaking-up and fine distribution of large and irregular-shape intermetallics in the matrix (including Al_3Ni and Mn-rich phases), dispersion strengthening effect of intermetallic dispersoids, work-hardening, and microstructural densification [22−26,36,37].

The substantial reduction of grain size to about 1 μm (Fig. 6) significantly contributes to alloy strength by grain boundary strengthening mechanism which is determined by the Hall−Petch equation [25,26,31]:

$$\sigma_g = \sigma_0 + kd^{0.5} \quad (6)$$

where σ_0 is the matrix friction stress and k is the Hall−Petch coefficient.

The high density of dislocations in the processed area also contributes to the alloy strengthening. The recrystallized grains are generally considered to have low density of dislocations [38]. However, it has been shown that some grains in the dynamically recrystallized zone contain high density of dislocations [35,39−41]. It has been also shown that [25] the SZ grains have a very high density of sub-boundaries, sub-grains, and dislocations, which in turn can effectively increase the matrix strength. The contribution of dislocations in the matrix strengthening can be evaluated by the following equation [32,42]:

$$\sigma_d = M\alpha Gb\rho^{0.5} \quad (7)$$

where M is the Taylor factor, α is a constant, G is the shear modulus, and ρ is the dislocation density.

The fracture and fine distribution of intermetallics in the FSPed alloys (Fig. 5) can also decrease the amplitude of the stress concentrated on the individual particles helping them to resist more against applied stresses before being fractured and/or de-bonded from the matrix. This, in turn, can reduce the possibility of micro-void formation from the fractured and/or de-bonded intermetallics and effectively retard the propagation of micro-cracks giving rise to a higher strength, hardness, ductility, and fracture toughness (Fig. 8).

Figure 12 shows the fracture surface morphologies corresponding to 4Ni1MnF and 4Ni4MnF samples, respectively. In agreement with the results of mechanical properties (Figs. 7 and 8), the fracture surface of 4Ni1MnF (Figs. 12(a, b) is extensively covered by fine and equiaxed dimples implying the initiation, growth, and coalescence of micro-voids in a high-energy ductile fracture process. The existence of fractured Mn-rich particles (Fig. 12(b)) at the bottom of dimples also suggests their critical role in impeding dislocations and the initiation of micro-cracks. Compared to 4Ni4Mn, increasing the area of dimpled fracture is quite evident on the fracture surface of 4Ni4MnF (Figs. 12(c, d)). The presence of fairly large Mn-rich particles is; however, evident on the fracture surface which is thought to be the reason for the lower ductility and fracture toughness in high-Mn sample.

FSP also almost eliminates the microstructural segregations and detrimental casting defects like bi-film oxides and micro-porosities. Figure 13 shows the OM microstructures of 4Ni4Mn in as-cast condition. The presence of micro-pores (Fig. 13(a)) and entrained bi-films (Fig. 13(b)) is quite evident in the microstructure. The micro-pores, which are generally originated from the precipitation of dissolved hydrogen and/or lack of efficient liquid feeding during solidification, act as potential stress risers and micro-cracks initiators [43,44], impairing the hardness and tensile properties. The

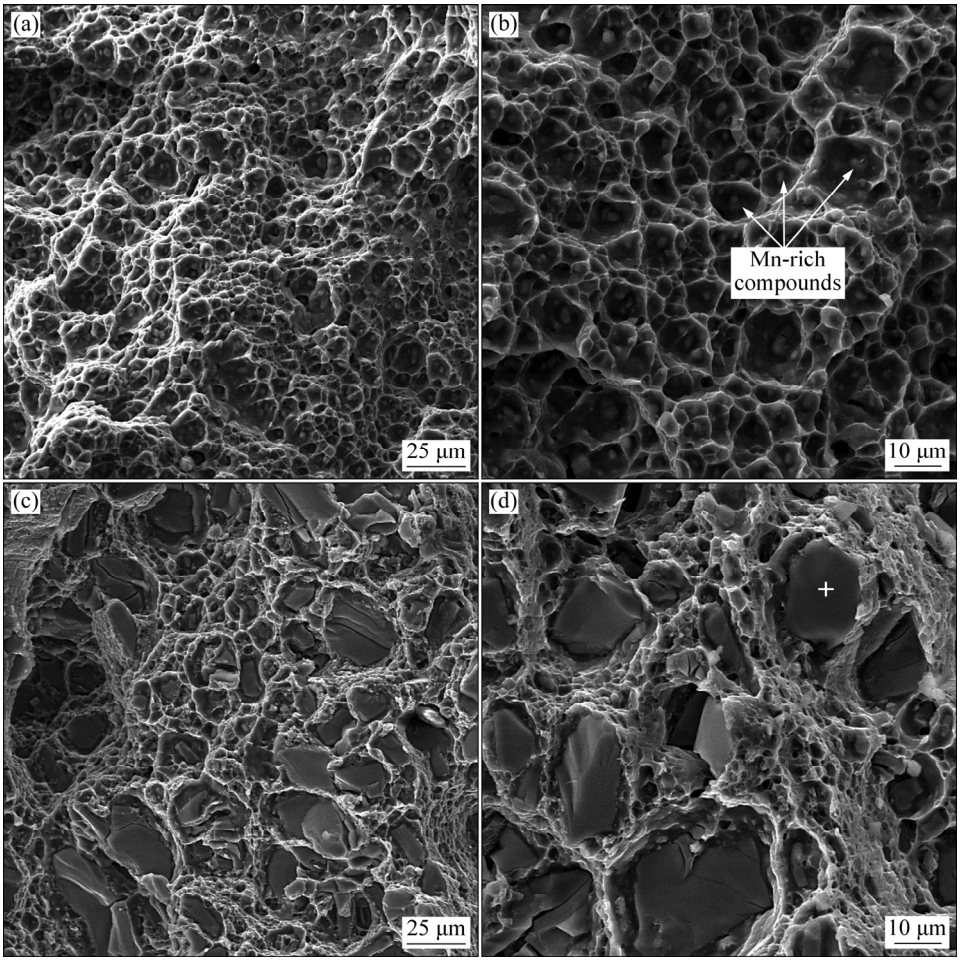

Fig. 12 SEM micrographs of fracture surfaces of 4Ni1MnF (a, b) and 4Ni4MnF (c, d)

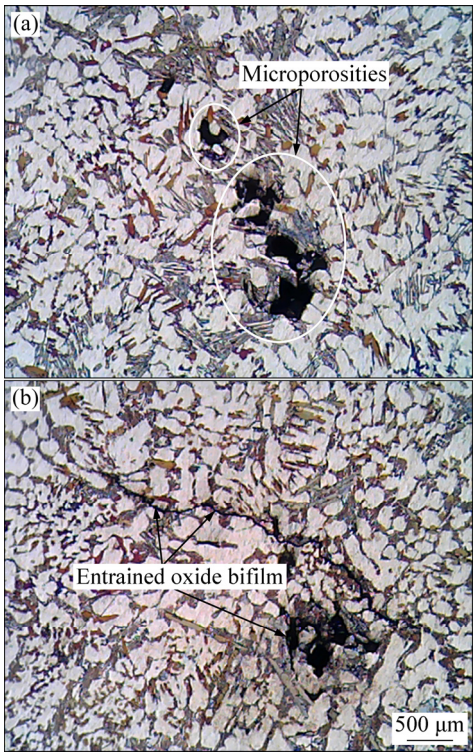

Fig. 13 OM micrographs showing presence of micro-porosities (a) and entrained bi-films (b) in as-cast 4Ni4Mn

entrained bi-films are also generally considered as pre-existing micro-cracks in the microstructure which significantly decrease tensile properties and reliability of castings [45−47]. During FSP, it seems that frictional heating and severe plastic deformation of the processed material effectively forge the existing micro-pores and convert the bi-film oxides to ultrafine oxide dispersoids in the microstructure, improving the tensile properties. The SEM of the fracture surface of FSPed samples (see Fig. 12) also reveals the formation of fine dimples on the surface implying their ductile fracture.

The variation of microhardness across the SZ perpendicular to the FSP direction is shown in Fig. 14. As seen, for a given Mn content, the SZ exhibits higher microhardness than the unaffected base metal (BM). This is while a large number of studies have demonstrated the SZ softening [22,25,48,49] due to phenomena such as coarsening and dissolution of the strengthening compounds, grains growth, and reduced strengthening effect of fragmented second-phase particles. Regarding to the non-heat treatable nature of Al−Ni−Mn alloys, the hardness increase of SZ can be due to the reduction of grain size and the elimination of casting defects during FSP.

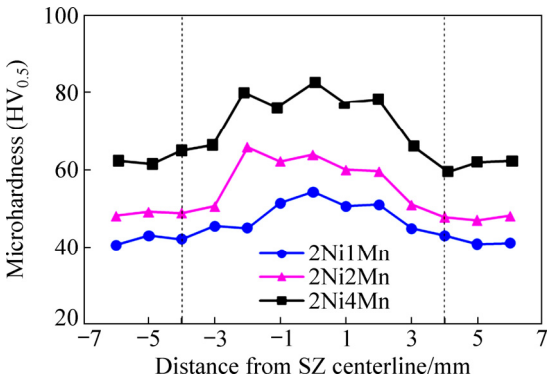

Fig. 14 Microhardness profiles of Mn-containing alloys at mid-thickness of their SZ perpendicular to FSP pin traverse direction

4 Conclusions

(1) The addition of Mn to Al−4Ni alloys leads to the precipitation of Mn-rich intermetallics in the matrix such as Al_6Mn and $Al_{60}Mn_{11}Ni_4$. The effective size, volume fraction, morphology, and distribution of these compounds are dependent on Mn concentration.

(2) FSP produces a homogenous microstructure comprised of ultrafine grains and finely distributed second-phase particles in a matrix, which have less density of micro-pores. The volume fraction of micropores and the average size of the primary particles in Al−4Ni−4Mn sample decreased from (3.11±1.62) and (47.18±9.29) μm in as-cast to about (0.64±0.11) and (2.75±2.26) μm in FSPed condition.

(3) Mn addition relatively increased the yield and tensile strength, but substantially decreased the fracture strain of the as-cast Al−4Ni alloy. This can be explained by its solid-solution strengthening effect and the impeding action of Mn-rich dispersoids on dislocations movement.

(4) After FSP, the tensile strength, yield strength, fracture strain, microhardness, and fracture toughness of 4Ni4MnF and 4Ni2Mn samples increased by 51%, 28%, 495%, 12%, and 850%, and by 67%, 30%, 230%, 20%, and 1185%, respectively. The most important mechanisms responsible for the improvement of mechanical properties are breaking-up and even distribution of Al_3Ni and Mn-rich intermetallics, dispersion strengthening effect of intermetallic dispersoids, formation of ultrafine-grained structure, work-hardening, microstructural densification, and elimination of large oxide bifilms.

References

[1] JAVIDANI M, LAROUCHE D. Application of cast Al–Si alloys in internal combustion engine components [J]. International Materials Review, 2014, 59(3): 132−158.

[2] KAUFMAN J G, ROOY E L. Aluminum alloy casting: properties, processes, and applications [M]. 1st ed. Materials Park, OH: ASM International, 1999: 7−20.

[3] LIMA J O, BARBOSA C R, MAGNO I A B, NASCIMENTO J M, BARROS A S, OLIVEIRA M C, SOUZA F A, ROCHA O L. Microstructural evolution during unsteady-state horizontal solidification of Al−Si−Mg (356) alloy [J]. Transactions of Nonferrous Metals Society of China, 2018, 28(6): 1073−1083.

[4] KOUTSOUKIS T, MAKHLOUF M M. An alternative eutectic system for casting aluminum alloys: I. Casting ability and tensile properties [J]. Light Metals, 2015: 277−282.

[5] LEE J A. Cast aluminum alloys for high temperature applications, in automotive alloys [C]//TMS Annual Meeting and Exhibition. NASA, Huntsville, USA: The Minerals, Metals & Materials Society, 2003: 1−8.

[6] LIN Y C, LUO S, JIANG X, TANG Y, CHEN M. Hot deformation behavior of a Sr-modified Al−Si−Mg alloy: Constitutive model and processing maps [J]. Transactions of Nonferrous Metals Society of China, 2018, 28(4): 592−603.

[7] FAN Y, MAKHLOUF M M. Castable aluminium alloys for high temperature applications [J]. Materials Science Forum, 2013, 765: 8−12.

[8] YU W, HAO Q, FAN L, LI J. Eutectic solidification microstructure of an Al−4Ni−2Mn alloy [J]. Journal of Alloys and Compounds, 2016, 688: 798−803.

[9] FAN Y, MAKHLOUF M M. The effect of introducing the Al−Ni eutectic composition into Al−Zr−V alloys on microstructure and tensile properties [J]. Materials Science and Engineering A, 2016, 654: 228−235.

[10] BELOV N A, ALABIN A N, ESKIN D G. Improving the properties of cold-rolled Al−6%Ni sheets by alloying and heat treatment [J]. Scripta Materialia, 2004, 50(1): 89−94.

[11] LIN J C, ZOLOTOREVSKY V S, GLAZOFF M V, MURTHA S J, BELOV N A. Al−Ni−Mn casting alloy for automotive and aerospace structural components: US Patent, 783730B2 [P]. 2001.

[12] SUWANPREECHA C, PANDEE P, PATAKHAM U, LIMMANEEVICHITR C. New generation of eutectic Al−Ni casting alloys for elevated temperature services [J]. Materials Science and Engineering A, 2018, 709: 46−54.

[13] MARTIN J W, DOHERTY R D, CANTOR B. Stability of microstructure in metallic systems [M]. Cambridge, UK: Cambridge University Press, 1997.

[14] HUNT W H Jr. New directions in aluminum based P/M materials for automotive applications [J]. Journal of Powder Metals, 2000, 36(6): 51−60.

[15] SAMPATH P, KRISHNA PARANGODATH V, UDUPA K R, KURUVERI U B. Fabrication of friction stir processed Al−Ni particulate composite and its impression creep behaviour [J]. Journal of Composites, 2015, 2015: 428630.

[16] PANDEY P, KASHYAP S, TIWARY C S, CHATTOPADHYAY K. Development of high-strength high-temperature cast Al−Ni−Cr alloys through evolution of a novel composite eutectic structure [J]. Metallurgical and Materials Transactions A, 2017, 48(12): 5940−5950.

[17] MU J, SHA P, ZHU Z, WANG Y, ZHANG H, HU Z. Synthesis of high strength aluminum alloys in the Al−Ni−La system [J]. Journal of Materials Research, 2014, 29(5): 708−717.

[18] KARAKÖSE E, KARAASLAN T, KESKIN M, UZUN O. Microstructural evolution and microhardness of a melt-spun Al−6Ni−2Cu−1Si (in wt.%) alloy [J]. Journal of Materials Processing and Technology, 2008, 195(1−3): 58−62.

[19] RAGAB M, SALEM H G. Investigation of the structural stability of nanostructured Al−5.7wt%−Ni mechanically alloyed eutectic alloy powder [J]. Light Metals, 2015: 346−352.

[20] DU Y, CHANG Y, HUANG B, GONG W, JIN Z, XU H. Diffusion coefficients of some solutes in fcc and liquid Al: Critical evaluation and correlation [J]. Materials Science and Engineering A, 2003, 363(1−2): 140−151.

[21] GONZALEZ G, LARA-RODRIGUEZ G A, SANDOVAL-JIMÉNEZ A, SAIKALY W, CHARAI A. The influence of cooling rate on the microstructure of an Al–Ni hypereutectic alloy [J]. Materials Characterization, 2008, 59(11): 1607−1612.

[22] MA Z Y. Friction stir processing technology: A review [J]. Metallurgical and Materials Transactions A, 2008, 39(3): 642−658.

[23] GAN W, ZHOU Z, ZHANG H, PENG T. Evolution of microstructure and hardness of aluminum after friction stir processing [J]. Transactions of Nonferrous Metals Society of China, 2014, 24(4): 975−81.

[24] CHEN Y, DIMG H, MALOPHEYEV S, KAIBYSHHEV R, CAI Z, YANG W. Influence of multi-pass friction stir processing on microstructure and mechanical properties of 7B04-O Al alloy [J]. Transactions of Nonferrous Metals Society of China, 2017, 27(4): 789−96.

[25] MISHRA R S, MA Z Y. Friction stir welding and processing [J]. Materials Science and Engineering R, 2005, 50(1−2):1−78.

[26] MA Z Y, SHARMA S R, MISHRA R S. Microstructural modification of as-cast Al−Si−Mg alloy by friction stir processing [J]. Metallurgical and Materials Transactions A, 2006, 37(11): 3323−3336.

[27] YANG Y, ZHAO Y, KAI X, TAO R. Super plasticity behavior and deformation mechanism of the in-situ Al_3Zr/6063Al composites processed by friction stir processing [J]. Journal of Alloys and Compounds, 2017, 710: 225−233.

[28] BARMOUZ M, ABRINIA K, KHOSRAVI J. Using hardness measurement for dislocation densities determination in FSPed metal in order to evaluation of strain rate effect on the tensile behavior [J]. Materials Science and Engineering A, 2013, 559: 917−919.

[29] EL-RAYES M M, EL-DANAF E A. The influence of multi-pass friction stir processing on the microstructural and mechanical properties of aluminum alloy 6082 [J]. Journal of Materials Processing and Technology, 2012, 212(5): 1157−1168.

[30] RYEN Ø, HOLMEDAL B, NIJS O, NES E, SJÖLANDER E, EKSTRÖM H E. Strengthening mechanisms in solid solution aluminum alloys [J]. Metallurgical and Materials Transactions A, 2006, 37(6): 1999−2006.

[31] SHAERI M H, SHAERI M, EBRAHIMI M, SALEHI M T, SEYYEDEIN S H. Effect of ECAP temperature on microstructure and mechanical properties of Al−Zn−Mg−Cu alloy [J]. Progress in Natural Science: Materials International, 2016, 26(2): 182−191.

[32] DARLING K A, ROBERTS A J, ARMSTRONG L, KAPOOR D, TSCHOPP M A, KECSKES L J. Influence of Mn solute content on grain size reduction and improved strength in mechanically alloyed Al−Mn alloys [J]. Materials Science and Engineering A, 2014, 589: 57−65.

[33] ZHAO Q, HOLMEDAL B, LI Y, SAGVOLDEN E, LØVVIK O M. Multi-component solid solution and cluster hardening of Al−Mn−Si alloys [J]. Materials Science and Engineering A, 2015, 625: 153−157.

[34] MUGGERUD A M F, MØRTSELL E A, LI Y, HOLMESTAD R. Dispersoid strengthening in AA3xxx alloys with varying Mn and Si content during annealing at low temperatures [J]. Materials Science and Engineering A, 2013, 567: 21−28.

[35] HUANG K T, LUI T S, CHEN L H. Effect of dynamically recrystallized grain size on the tensile properties and vibration fracture resistance of friction stirred 5052 alloy [J]. Materials Transactions, 2006, 47(9): 2405−2412.

[36] BARUCH L J, RAJU R, BALASUBRAMANIAN V, RAO A G, DINAHARAN I. Influence of multi-pass friction stir processing on microstructure and mechanical properties of die cast Al−7Si−3Cu aluminum alloy [J]. Acta Metallurgica Sinica (English letters), 2016, 29(5): 431−440.

[37] DINAHARAN I, ASHOK KUMAR G, VIJAY S J, MURUGAN N. Development of Al_3Ti and Al_3Zr intermetallic particulate reinforced aluminum alloy AA6061 in situ composites using friction stir processing [J]. Materials and Design, 2014, 63: 213−222.

[38] HUMPHREYS F J, HATHERLY M. Recrystallization and related annealing phenomena [M]. 2nd ed. Killington, Oxford, UK: Elsevier Ltd, 2004.

[39] SATO Y S, PARK S H C, KOKAWA H. Microstructural factors governing hardness in friction-stir welds of solid-solution-hardened Al alloys [J]. Metallurgical and Materials Transactions A, 2001, 32(12): 3033−3042.

[40] JATA K V, SANKARAN K K, RUSCHAU J J. Friction-stir welding effects on microstructure and fatigue of aluminum alloy 7050-T7451 [J]. Metallurgical and Materials Transactions A, 2000, 31(9): 2181−2192.

[41] HUANG K T, LUI T S, CHEN L H. Pre-treated effect of friction stir processing of Al Alloy 5052 on vibration fracture behavior under resonant vibration [J]. Materials Transactions, 2005, 46(12): 3051−3058.

[42] PANIGRAHI S K, JAYAGANTHAN R. Influence of solutes and second phase particles on work hardening behavior of Al 6063 alloy processed by cryorolling [J]. Materials Science and Engineering A, 2011, 528(7−8): 3147−3160.

[43] LUDWIG T, DI SABATINO M, ARNBERG L, DISPINAR D. Influence of oxide additions on the porosity development and mechanical properties of A356 aluminium alloy castings [J]. International Journal of Metalcasting 2012, 6: 41−50.

[44] MUGICA G W, TOVIO D O, CUYAS J C, GONZÁLEZ A C. Effect of porosity on the tensile properties of low ductility aluminum alloys [J]. Materials Research 2004, 7: 221−229.

[45] AKABERI N, TAGHIABADI R, RAZAGHIAN A. Effect of bifilm oxides on the dry sliding wear behavior of Fe-rich Al–Si alloys [J]. Journal of Tribology, 2017, 139: 51602.

[46] CAMPBELL J. An overview of the effect of bifilms on the structure and properties of cast alloys [J]. Metallurgical and Materials Transactions B, 2006, 37(6): 857−863.

[47] BOZCHALOEI G E, VARAHRAM N, DAVAMI P, KIM S K. Effect of oxide bifilms on the mechanical properties of cast Al−7Si−0.3Mg alloy and the roll of runner height after filter on their formation [J]. Material Science and Engineering A, 2012, 548: 99−105.

[48] KWON Y J, SHIGEMATSU I, SAITO N. Production of ultra-fine grained aluminum alloy using friction stir process [J]. Materials Transactions, 2003, 44: 1343−1350.

[49] EL-RAYESA M M, EL-DANAF E A. The influence of multi-pass friction stir processing on the microstructural and mechanical properties of Aluminum Alloy 6082 [J]. Journal of Materials Processing Technology, 2012, 212: 1157−1168.

通过搅拌摩擦加工提高含锰亚共晶 Al−4Ni 合金的力学性能

Fatemeh YOUSEFI, Reza TAGHIABADI, Saeid BAGHSHAHI

Department of Materials Science and Metallurgy, Imam Khomeini International University (IKIU), Qazvin, Iran

摘　要：研究锰加入量(1 wt.%、2 wt.%、4 wt.%)和搅拌摩擦加工(FSP)对 Al−4Ni 合金显微组织和力学性能的影响。结果表明，锰促进了 Al_6Mn 和 $Al_{60}Mn_{11}Ni_4$ 金属间化合物的形成。这些富锰化合物提高了合金的强度和硬度，但降低了其延性和断裂韧性。为了提高延性和韧性，对铸态合金进行搅拌摩擦加工(转速为 1600 r/min、横移速度为 12 mm/min)。结果表明，FSP 大大改善了材料的力学性能，合金的抗拉强度、屈服强度、断裂应变、显微硬度和断裂韧性分别提高了 67%、30%、230%、20%和 1185%。研究发现，富锰化合物的细化再分布、超细晶粒的形成、显微结构致密化以及铸件微孔和氧化双膜等缺陷的消除是提高合金力学性能重要的因素。断口形貌研究表明，铸态富锰合金为脆性断裂模式，其断口含微解理面，而搅拌摩擦加工后的合金为韧性断裂，其断口含细小的等轴韧窝。

关键词：搅拌摩擦加工；铝镍合金；锰；金属间化合物；力学性能

(Edited by Xiang-qun LI)